

# Imaging subcellular scattering contrast by using combined optical coherence and multiphoton microscopy

Shuo Tang

Department of Electrical and Computer Engineering, University of British Columbia, Vancouver V6T 1Z4, Canada, and Beckman Laser Institute, University of California, Irvine, California 92612, USA

Chung-Ho Sun, Tatiana B. Krasieva, Zhongping Chen, and Bruce J. Tromberg

Beckman Laser Institute, University of California, Irvine, California 92612, USA

Received October 12, 2006; revised November 22, 2006; accepted November 27, 2006; posted December 6, 2006 (Doc. ID 76024); published February 2, 2007

The structural origin of scattering contrast from single cells is examined by using a combined optical coherence and multiphoton microscope based on a 12 fs Ti:sapphire source and a 0.95 NA objective. High-resolution coherence-gated scattering images from single cells are coregistered and compared with two-photon-excited fluorescence images. Scattering contrast is observed from mitochondria, plasma membrane, actin filaments, and the boundary between cytoplasm and nucleus. There is little contribution to scattering from regions inside the nuclear core. These results confirm that light scattering signals from specific subcellular structures can be visualized by using coherent reflectance geometry. © 2007 Optical Society of America

OCIS codes: 170.0180, 170.4500, 180.2520, 170.3660, 290.0290.

Near-infrared light scattering in tissues is dominated by microscopic particles in cells and structural proteins in the extracellular matrix. However, the precise structural origins of light scattering in tissues are not well understood. Beauvoit *et al.*<sup>1</sup> measured hepatocytes and mitochondria by using time-resolved scattering spectroscopy and discovered that mitochondria were the primary contributors to light scattering. From the angular dependence of polarized light scattering in epithelial cells and isolated nuclei, Mourant *et al.*<sup>2</sup> determined that the size distribution of scattering structures ranged from 2  $\mu\text{m}$  to 10 nm or less. However, a limitation of these elastic scattering spectroscopy measurements is that microscopic scattering centers and scatter sizes must be identified and derived indirectly from measurements based on bulk suspensions.

By imaging single hepatocytes and breast tumor cells with confocal reflectance microscopy, Drezek *et al.*<sup>3</sup> observed that there was little intrinsic scattering contrast from subcellular structures but that the nuclear contrast could be selectively increased by adding acetic acid. Optical coherence tomography (OCT) images of *Xenopus laevis* and human esophagus epithelium with imaging areas of hundreds of micrometers have shown strong scattering from plasma membranes and nuclei.<sup>4,5</sup> However, high-NA OCT imaging on the single-cell level has not been reported, and small scattering centers other than the plasma membrane and nucleus have not been identified.

In this Letter, we utilize a combined OCT and multiphoton microscopy (MPM) system to study scattering contrast in single cells. Combined MPM–OCT can acquire coregistered two-photon-excited fluorescence (TPEF) and backscattered light simultaneously from the same sampling volume.<sup>6–8</sup> This allows the use of fluorescence targeted probes to identify molecular components of subcellular scattering structures. De-

tails of the combined MPM–OCT system used in our experiment are described in Ref. 6. Briefly, a 12 fs Ti:sapphire laser (Femtolasers) excites MPM and OCT signals simultaneously. The MPM and OCT channels have matched transverse resolutions (0.5  $\mu\text{m}$ ) and axial resolutions<sup>6</sup> (1.5  $\mu\text{m}$ ). The frame rate of the system is 0.15 Hz. A 0.95 NA water-immersion objective illuminates and collects light in a full cone angle of 92°. Because the signals are collected in a backward geometry, the scattering angle collected is from 88° to 180°.

To develop a realistic three-dimensional (3D) tissue matrix, we embedded human glioblastoma cells in a Matrigel matrix (BD Biosciences). Matrigel is a solubilized basement membrane matrix. Embedding the cells in Matrigel creates a natural 3D extracellular matrix environment for the cells to grow and maintain normal activity. In addition, the cells are mounted for 3D scanning and lifted above the glass surface to avoid OCT background. In this work, we used several fluorescent vital dyes on live cells to label subcellular organelles, including DAPI (Invitrogen) for nuclei, Rhodamine 123 (Invitrogen) for mitochondria, and PKH67 (Sigma) for plasma membrane. Furthermore, Alexa Fluor 488 conjugated to phalloidin (Invitrogen) is used to target actin filaments in fixed cells.

Typical TPEF and OCT images of glioblastoma cells are shown in Fig. 1. Each row represents one cell, with the corresponding TPEF, OCT, and merged images displayed in the left, middle, and right columns. These images are minimally processed to adjust contrast, and the merged images are color coded in green for TPEF and red for OCT channels. Overlapping pixels are displayed in yellow. Figures 1(a)–1(c) show the signals from an unlabeled cell. The scattering pattern of this cell has a well-organized structure, as shown in Fig. 1(b). The cell

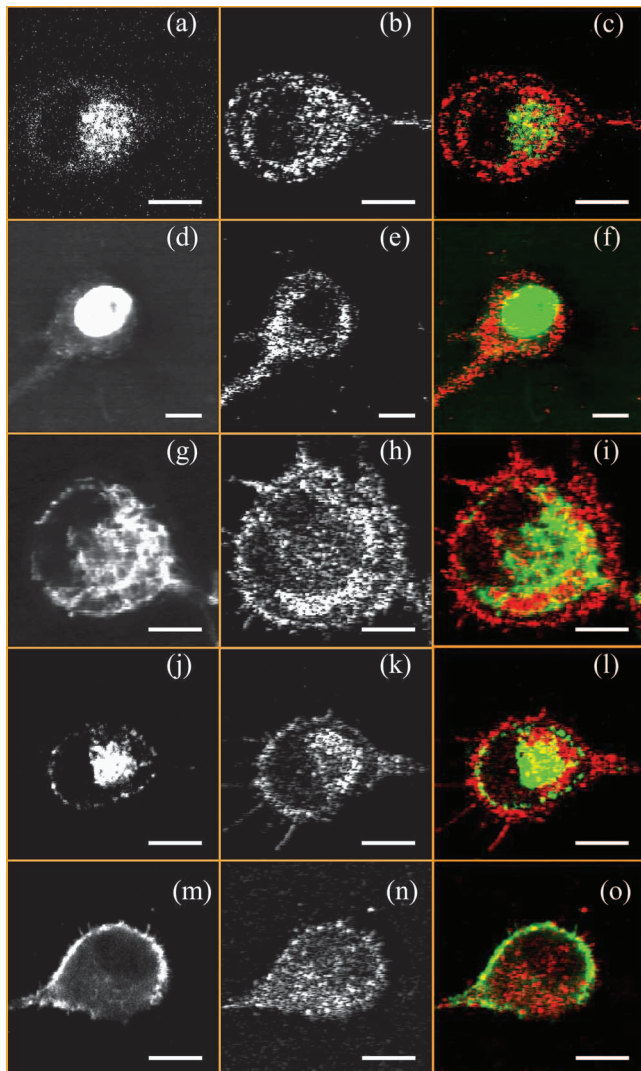


Fig. 1. Comparison of TPEF (left), OCT (middle), and merged (right) images of single cells. (a)–(c) Single cell without labeling; (d)–(f) with DAPI labeling for nuclei; (g)–(i) with Rhodamine 123 labeling for mitochondria; (j)–(l) with PKH67 labeling for plasma membrane; (m)–(o) with Alexa Fluor 488 conjugated to phalloidin for actin filaments. In the merged images, TPEF and OCT signals are in green and red, respectively. The scale bar is 10  $\mu\text{m}$ .

shows an outer ring surrounding a central body within which there is a dark area of relatively low scattering. A cluster of bright scattering centers is located adjacent to the dark area. The corresponding TPEF image is shown in Fig. 1(a). The TPEF signal is the autofluorescence mainly from the cytoplasm due to mitochondrial fluorescence. The merged image is shown in Fig. 1(c) with the distinctive regions matched in the two channels. The weakly fluorescent nuclear region matches the low scattering dark area in the center of the cell. The bright autofluorescence region in the cytoplasm matches the bright scattering cluster area. The bright scattering pattern in the outer ring does not have a corresponding autofluorescence signature.

Cells labeled with DAPI are imaged to identify the nuclear area, and the images are shown in Figs. 1(d)–1(f). In Fig. 1(d) the nucleus is clearly revealed

by the bright DAPI fluorescence. In the merged image the area of DAPI fluorescence matches well with the dark area of low light scattering in OCT. This confirms that the low scattering area coincides with the nuclear core area. However, on the rim of the nucleus, there is overlap between the nuclear staining and the bright scattering signal, which is believed to be a result of the refractive index heterogeneity between the cytoplasm and the nucleus. Figures 1(g)–1(i) show a cell labeled with the mitochondrial vital dye. In Fig. 1(g), the TPEF image indicates that there are many mitochondria that are distributed throughout the cytoplasm. In the merged image the bright scattering area in the cytoplasm matches well with the mitochondrial distribution.

Figures 1(j)–1(l) show images of a cell stained with PKH67 plasma membrane dye. In Fig. 1(j) plasma membrane fluorescence is clearly visible. A large portion of the dye is also found inside the cell, because the metabolism of the cell internalizes the dye. Along the plasma membrane region, bright scattering signals are observed as shown in Fig. 1(l). Because the thickness of the plasma membrane is below the resolution of the system, other structures underlying the plasma membrane can also contribute to the scattering signals within the resolution volume. Figures 1(m)–1(o) show images of a cell stained for actin filaments. Figure 1(m) shows actin filaments concentrated along the cell cortex right below plasma membrane and actin filopodia reaching out on the cell surface. It is observed that the distribution of actin filaments is colocalized with the bright scattering on the cell surface within the resolution of the system. The actin filopodia are shown to be highly scattering in the OCT image.

Figures 2(a)–2(k) show a series of OCT image sections from a single cell separated by 1  $\mu\text{m}$  steps in the  $Z$  direction. As the focused laser beam scans the top of the cell, scattering is observed from the plasma membrane and the associated actin filaments. When the laser beam scans a middle section of the cell, a

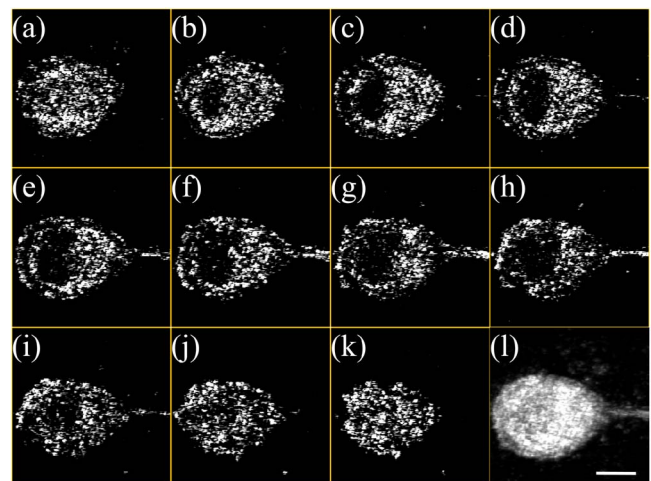


Fig. 2. (Color online) Multiple frames of OCT images of a single cell optically sliced from the top to the bottom. From (a) to (k), the images are taken at progressive 1  $\mu\text{m}$   $Z$  steps. (l) is the XY projection of the whole  $Z$  stack of cell slices. The scale bar is 10  $\mu\text{m}$ .

patterned structure is observed that reveals a weak nuclear signal and strong scattering from mitochondria. When the laser beam focuses on the bottom of the cell, the structured pattern disappears, and scattering from the cell surface appears again. The *XY* projection of the stack of images is shown in Fig. 2(l) as a comparison. When all the images are summed up and averaged in the projection, the fine structures of scattering are lost. Therefore it is important to have ultrahigh resolution in order to see subcellular scattering contrast.

Quantitative data are further analyzed from 21 cells, including 13 human glioblastoma cells, 3 neonatal foreskin fibroblasts, and 5 rat kangaroo kidney epithelium cells. Within the 21 cells, 7 cells each are stained for mitochondria, actin filaments, and nuclei, respectively. The images are analyzed with IPLab (BD Biosciences). First the normalized mean scattering intensity is quantified. For example, the TPEF image is segmented to define the region of mitochondria. This segmentation is then transferred to the corresponding OCT image to mark out the mitochondrial region. The OCT intensity is averaged over the mitochondrial region to get the mean mitochondrial scattering intensity, which is further normalized to the average scattering intensity of the whole cell. The normalized mean scattering intensity in the mitochondrial region is found to be  $0.79 \pm 0.06$ . In comparison, the normalized mean scattering intensities in the actin filament and the nuclear regions are  $0.79 \pm 0.05$  and  $0.35 \pm 0.10$ , respectively. Therefore mitochondria and actin filaments are observed to be twice as scattering as the nuclei when probed with a focused laser beam in a backward geometry.

Second, the normalized area of scattering is also calculated. For instance, the TPEF and OCT images are segmented to define the mitochondrial and the scattering areas. The overlapping area between the two segments is defined as the scattering mitochondrial area. This scattering mitochondrial area is then normalized to the total mitochondrial area. In the analysis,  $(0.63 \pm 0.04) \times 100\%$  of the mitochondrial area is found to have bright scattering signals. In comparison,  $(0.64 \pm 0.04) \times 100\%$  and  $(0.17 \pm 0.07) \times 100\%$  of the actin and nuclear areas are scattering, respectively. Therefore it is shown that the majority of the mitochondrial and actin areas are scattering but that little of the nuclear area is scattering.

No significant difference in the scattering properties is observed, and the above characteristics are common to all three cell types. The statistics are summarized in Table 1. Systematic errors introduced by the speckle noise and the slow demodulation speed of the OCT channel are the main reasons that the fluorescence-scattering correlation values are not optimum. Data from the plasma membrane staining are not used in the quantitative analysis because the dye is not localized in plasma membrane only.

In our experiment, the focused laser beam probes the heterogeneity of the refractive index in cells on the scale of the system resolution. We have observed high scattering contrast from mitochondria, plasma membrane, actin filaments, and the boundary be-

**Table 1. Normalized Mean Scattering Intensity and Scattering Area by Region<sup>a</sup>**

Region	Mean Scattering Intensity	Scattering Area ( $\times 100\%$ )
Mitochondria	$0.79 \pm 0.06$	$0.63 \pm 0.04$
Actin Filaments	$0.79 \pm 0.05$	$0.64 \pm 0.04$
Nuclei	$0.35 \pm 0.10$	$0.17 \pm 0.07$

<sup>a</sup>Data are averaged over 7 cells, each stained for mitochondria, actin filaments and nuclei, respectively, with a total of 21 cells.

tween cytoplasm and nucleus. These regions have a high heterogeneity of refractive index on the  $\sim 1 \mu\text{m}$  scale because of densely packed lipids, proteins, and nucleic acids. In our study the nuclear core area has been found to have relatively lower scattering than the cytoplasm, which we believe is because of our probing geometry. Nuclei tend to have smaller scattering angles compared with mitochondria and actin filaments, but angles smaller than  $88^\circ$  are not detected in our system. Furthermore, when probed with a focused laser beam, the nucleus should not be looked at as a single particle but as an organelle structure. Its heterogeneity is mainly on the boundary between cytoplasm and nucleus but with little variation inside the nucleus, likely due to the quasi-uniform distribution of chromatin and proteins.

In conclusion, we have investigated the scattering origins of subcellular structures by using a combined MPM-OCT system. High scattering contrast has been observed from mitochondria, plasma membrane and associated actin filaments, and the boundary between cytoplasm and nucleus. This method can be used to improve our understanding of the microscopic origins of scattering contrast in cells and extracellular matrix and possibly to enhance contrast in tissue optical imaging.

This work was supported by the National Institutes of Health (LAMMP-P41RR01192), National Cancer Institute (CA-91717), and the Air Force Office of Scientific Research (MFEL FA9550-04-1-0101). B. J. Tromberg's e-mail address is [bjtrombe@uci.edu](mailto:bjtrombe@uci.edu).

## References

1. B. Beauvoit, T. Kitai, and B. Chance, *Biophys. J.* **67**, 2501 (1994).
2. J. R. Mourant, T. M. Johnson, S. Carpenter, A. Guerra, T. Aida, and J. P. Freyer, *J. Biomed. Opt.* **7**, 378 (2002).
3. R. Drezek, M. Guillaud, T. Collier, L. Boiko, A. Malpica, C. Macaulay, M. Follen, and R. Richards-Kortum, *J. Biomed. Opt.* **8**, 7 (2003).
4. S. A. Boppart, B. E. Bouma, C. Pitris, J. F. Southern, M. E. Brezinski, and J. G. Fujimoto, *Nat. Med.* **4**, 861 (1998).
5. A. Dubois, K. Grieve, G. Moneron, R. Lecaque, L. Vabre, and C. Boccara, *Appl. Opt.* **43**, 2874 (2004).
6. S. Tang, T. B. Krasieva, Z. P. Chen, and B. J. Tromberg, *J. Biomed. Opt.* **11**, 020502 (2006).
7. E. Beaupaire, L. Moreaux, F. Amblard, and J. Mertz, *Opt. Lett.* **24**, 969 (1999).
8. C. Vinegoni, T. Ralston, W. Tan, W. Luo, D. L. Marks, and S. A. Boppart, *Appl. Phys. Lett.* **88**, 053901 (2006).